Self-assembly in block polyelectrolytes

Shuang Yang, Aleksey Vishnyakov, and Alexander V. Neimark[a)]
Department of Chemical and Biochemical Engineering, Rutgers, The State University of New Jersey, 98 Brett Road, Piscataway, New Jersey 08854, USA

(Received 15 September 2010; accepted 7 December 2010; published online 1 February 2011)

The self-consistent field theory (SCFT) complemented with the Poisson–Boltzmann equation is employed to explore self-assembly of polyelectrolyte copolymers composed of charged blocks A and neutral blocks B. We have extended SCFT to dissociating triblock copolymers and demonstrated our approach on three characteristic examples: (1) diblock copolymer (AB) melt, (2) symmetric triblock copolymer (ABA) melt, (3) triblock copolymer (ABA) solution with added electrolyte. For copolymer melts, we varied the composition (that is, the total fraction of A-segments in the system) and the charge density on A blocks and calculated the phase diagram that contains ordered mesophases of lamellar, gyroid, hexagonal, and bcc symmetries, as well as the uniform disordered phase. The phase diagram of charged block copolymer melts in the charge density – system composition coordinates is similar to the classical phase diagram of neutral block copolymer melts, where the composition and the Flory mismatch interaction parameter χ_{AB} are used as variables. We found that the transitions between the polyelectrolyte mesophases with the increase of charge density occur in the same sequence, from lamellar to gyroid to hexagonal to bcc to disordered morphologies, as the mesophase transitions for neutral diblocks with the decrease of χ_{AB}. In a certain range of compositions, the phase diagram for charged triblock copolymers exhibits unexpected features, allowing for transitions from hexagonal to gyroid to lamellar mesophases as the charge density increases. Triblock polyelectrolyte solutions were studied by varying the charge density and solvent concentration at a fixed copolymer composition. Transitions from lamellar to gyroid and gyroid to hexagonal morphologies were observed at lower polymer concentrations than the respective transitions in the similar neutral copolymer, indicating a substantial influence of the charge density on phase behavior. © *2011 American Institute of Physics*. [doi:10.1063/1.3532831]

I. INTRODUCTION

Polyelectrolytes composed of immiscible charged and neutral blocks are widely used in modern nanotechnologies for producing drug delivery capsules, perm-selective barrier films, fuel cell membranes, nanostructured coatings and separators, as well as templates for various mesoporous materials.[1–4] The unique properties of polyelectrolytes and polyelecrolyte-based materials are determined, to a great extent, by a variety of regular mesophases assumed by block copolymer melts and solutions. Depending on the composition and temperature, block copolymers tend to self-assemble into ordered structures of different crystallographic symmetries forming lamellar layers, hexagonal cylindrical arrays, gyroid bicontinuous networks, and ordered three-dimensional structures, like spherical micelles positioned at the sites of body-centered cubic (BCC) lattice.[1] While the self-assembly and morphological transitions between different mesophases are well documented experimentally in both neutral and charged block copolymer systems, most of theoretical and simulation models addressed neutral systems that were thoroughly investigated.[5] The phase equilibrium of neutral diblock melt depends on two parameters—the composition or fraction of one of the blocks and the interaction mismatch between the blocks χ_{AB}, which depend on temperature. By changing any of these parameters keeping the other fixed, it is possible to drive the system from one stable mesophase to another. In particular, it was established that in the weak segregation regime, a reduction of the Flory mismatch interaction parameter between the blocks χ_{AB} or an increase of temperature may induce lamellar-to-gyroid (L→G), gyroid-to-hexagonal (G→H), hexagonal-to-cubic (H→C), and cubic-to-disordered (C→D) phase transitions in AB diblock and ABA triblock copolymers with different length of A and B segments.[6,7] Leibler[7] proposed a Landau mean field approach to analyze the mesophase separation and transitions between ordered and "disordered" mesophases of neutral diblock copolymer melts. Later, Mayes and de la Cruz[8] extended this analysis to triblock copolymers and star copolymer melts. Their results show that when drawn in composition—temperature or composition—$1/\chi_{AB}$ coordinate planes, the L-G, G-H, H-BCC, and BCC-D transition boundaries form bowl-shaped curves one above another. All these curves merge at a single "critical" common point (T^c, f^c), or (χ^c_{AB}, f^c_A), where the free-energies of all five phases (L, G, H, cubic BCC, and D) are equal. For symmetric diblocks,[6] this point corresponds to the maximum of the boundary curves and it represents the critical point in the mean field sense. This critical point corresponds to a

a)Author to whom correspondence should be addressed. Electronic mail: aneimark@rci.rutgers.edu.

second order order–disorder structural transition, which occurs at $f_A = 0.5$ upon decreasing χ_{AB} (or increasing T) directly from lamellar mesophase L to the uniform disordered phase D, without the intermediate L→G, G→H, H→BCC, and BCC→D transitions. At other compositions beyond the critical one, the order–disorder *first order* phase transition occurs from the BCC mesophase. For triblock copolymers[8–10] and asymmetric diblock copolymers,[11,12] the phase diagram is tilted. The critical point composition does not equal 0.5 $f_A^c \neq 0.5$, and it does not correspond to the maximum of order–disorder transition boundary. Later, Fredrickson and Helfand[13] and Mayes and de la Cruz[14] accounted for the concentration fluctuation correction and concluded that block copolymer melts undergo a first order transition rather than the second order transition predicted by the mean field theory. They found that the chain length N should be considered as an additional parameter determining the phase behavior. For finite N, they identified finite width composition intervals, within which the order–disorder transition occurs directly from either lamellar or hexagonal mesophases without an intermediate transition into BCC ordered mesophase. Since we use a mean field approximation, the mean field results of Refs. 6 and 8 serve as references for our studies.

Attempts to consider the electrostatic effects in block polyelectrolytes are quite limited. Accounting for the long-range electrostatic interactions remains challenging within theoretical approaches based on comparison of free-energy of different morphologies, such as the random phase approximation (RPA),[15,16] or self-consistent field theory (SCFT),[16–18] as well as with computer simulations performed with Monte Carlo,[19] coarse-grained molecular dynamics,[20] and MesoDyn, a mesoscale dynamic density functional theory (DDFT)[21,22] where the system morphology is unconstrained. Marko and Rabin[23] investigated the phase stability of diblock copolymer melts composed of charged A and neutral B blocks. Following Leibler's method,[7] the authors used RPA to calculate the free-energy and concluded the charge increase reduces the stability of ordered phases. This effect was associated with the translational entropy of counterions. Recently, Kumar and Muthukumar[16] employed the RPA and SCFT methods for predicting the stability limit and transition boundaries between different ordered mesophases in charged-neutral diblock salt-free melts. Both methods, RPA and SCFT, showed a near-perfect agreement in determining the disordered phase stability; however, the SCFT calculations were limited to the lamellar geometry. In general, the charged-neutral diblocks were found less ordered than the neutral–neutral diblocks with the same Flory mismatch interaction parameter χ_{AB}. Qualitatively, an increase in charge density of A block had a similar effect on the morphology as a reduction of the parameter χ_{AB}.

A similar trend was obtained by Kyrylyuk and Fraaije,[21] who extended the MesoDyn method onto polyelectrolyte solutions and applied it to predict the phase behavior of ABA triblock polyelectrolytes in the presence of solvent, which is miscible with A blocks. Increased charge density of the hydrophilic end block was found to drive the system to change morphologies in L→G→H→BCC→D direction, as a reduction of the Flory mismatch interaction parameter χ_{AB} would in neutral systems. The treatment of electrostatic interactions in that work was based on the Donnan approximation, which assumes that the net charge at any lattice site is exactly zero. The Donnan approximation is accurate at a high ionic strength, which in this case essentially means that the Debye length is much smaller than the characteristic mesophase segregation scale. It should be noted that the phase behavior of triblock copolymers studied by Kyrylyuk and Fraaje[21] differs substantially from that of diblocks, especially in the presence of solvent, while an early study of neutral block copolymers of Helfand and Wasserman[24] concluded that melts of strongly segregating ABA triblock and AB diblock copolymers with the same A fraction behave very similarly. Later, Mayes and de la Cruz[8] found that the phase diagram of triblock copolymer melts is highly asymmetric, and SCFT modeling of Matsen[25] and Matsen and Thompson[9] showed the importance of bridged configurations in ABA triblock systems. These configurations, where A blocks that belong to the same chain are located in different A-rich domains, do not exist in diblock copolymers. Concluding this overview, it is worth noting that despite some progress in understanding of the role of electrostatic interactions on self-assembly of block polyelectrolyte, a charge-dependent phase diagram of the transition boundaries between different mesophase morphologies, similar to that established for neutral block copolymers, is still unavailable. Specifics of self-assembly depend on a delicate balance between different competing factors including chain conformational entropy, thermodynamic incompatibility of unlike blocks, translational entropy of small ions, and long-range electrostatic interactions. To address these challenges, it is necessary to build a comprehensive theory of thermodynamic equilibrium and stability of ordered block polyelectrolyte mesophases focusing on the effects of electrostatic interactions in salt-free and salt systems.

In this paper, we employ the SCFT of polyelectrolytes complemented with the Poisson–Boltzmann equation to explore the self-assembly of copolymers composed of charged A and neutral B blocks. In Sec. II, we present the proposed SCFT approach to analyzing the phase behavior of diblock and triblock copolymer melts and solutions. This approach is based on the theory of polyelectrolyte systems developed by Shi and Noolandi[17] and Wang *et al.*[18] and it was earlier used by Kumar and Muthukumar[16] for analyses of lamellar mesophases of diblock polyectrolyte melts. In Sec. III A, we examine the influence of electrostatic interactions on the phase behavior of charged diblock and triblock copolymers in salt-free melts. In Sec. III B, we perform SCFT calculations of charged ABA triblock polyelectrolyte copolymer self-assembly in a salt solution. A summary of results and conclusions are given in Sec. IV.

II. THEORETICAL FRAMEWORK

In this work, we consider AB diblock and ABA triblock copolymers in salt-free melt and in aqueous salt solution. A block represents a polyelectrolyte, that is, it contains polar groups that dissociate forming anions bonded to the polymer surrounded by mobile cations. B block is neutral. A

typical example of such systems are sulfonated polystyrene-(ethylene-butylene)-styrene triblock copolymers (sSEBS).[26] The system is considered in the canonical ensemble at fixed temperature T, volume V, and given numbers of: n_p polymer chains, n_S neutral solvent molecules (S), n_I counterions released from dissociated A blocks, and $n_\pm$ positive and negative ions of dissolved salt. Polymer chains are considered as formed by coarse-grained Kuhn's segments. The length of the chain is $N = N_A + N_B$ for diblock copolymer and is $N = 2N_A + N_B$ for triblock copolymer. N_A and N_B are the numbers of A and B segments in the respective blocks. The chain composition f_A is defined as the fraction of A blocks: $f_A = N_A/N$ (diblock) or $f_A = 2N_A/N$ (triblock). For simplicity, we assume that A and B segments have the same Kuhn length b, and the solvent beads have the same size b. Note that the solvent bead of size b includes several water molecules. The volume densities are defined in units related to the Kuhn's segment length b. The system is assumed incompressible, and the charges are smeared over and equally distributed over A segments with an equal charge density, or degree of ionization, denoted by p. The volumes of the ions are neglected so that they do not contribute into Flory– Huggins repulsion interactions. The electrolyte solution is characterized by the Bjerrum length, $l_B = e^2/4\pi\varepsilon_r\varepsilon_0 k_B T$, at which the electrostatic potential equals the thermal motion energy; ε_0 is the vacuum permittivity and ε_r is the relative dielectric constant of the medium. It is worth noting that in general, the dielectric constant depends on the local concentrations of polymer segments and solvent molecules that may have a significant effect on long-range electrostatic interactions in some cases.[18] In our calculations, we set $\varepsilon_r \approx 20$ that is a typical value assumed in literature for polymer systems.[23]

The SCFT is based on Edwards' Hamiltonian for flexible polymer chains.[27,28] A detailed description of SCFT of polyelectrolyte solutions is given in Ref. 17. In the SCFT approach, the complex interactions between all molecules are decoupled using the mean field approximation. For each component, j, an effective external mean field, ω_j, is introduced to model the averaged interaction of this component j with all other components of the system. In the mean field approximation, the free-energy of the system F is presented as the following sum:[17]

$$\frac{F}{\rho_0 k_B T} = \int_V d\mathbf{r}\Big\{\chi_{AB}\phi_A\phi_B + \chi_{AS}\phi_A\phi_S + \chi_{BS}\phi_B\phi_S - \sum_j \phi_j\omega_j\Big\} - \frac{V\bar{\phi}_p}{N}\ln\left(\frac{Q_p}{\bar{\phi}_p}\right) - \sum_{i=S,I,\pm} V\bar{\phi}_i \ln\left(\frac{Q_i}{\bar{\phi}_i}\right) + \int_V d\mathbf{r}\Big[p\phi_A + Z_+\phi_+ + Z_I\phi_I + Z_-\phi_-)\varphi_e - \frac{b^2}{2\tau}|\nabla\varphi_e|^2\Big]. \quad (1)$$

Here, the summation by j runs over all components (A,B,S,I,+,−) and i runs only over small molecules (S,I,+, −). χ_{AS} and χ_{BS} are the Flory parameters of A–S and B–S segment–segment interactions, respectively. Z_I, Z_+, Z_- are the valence number of respective ions. ϕ_j is the respective volume fractions. Q_p is the partition function of a polymer chain in the mean fields ω_A, ω_B. Q_i is the partition function of a small molecule of type i in the mean field ω_i. φ_e is the dimensionless electrostatic potential. The bulk volume fraction of polymer segments is $\bar{\phi}_p = n_p N b^3/V$. For the solvent, $\bar{\phi}_S = n_S b^3/V = 1 - \bar{\phi}_p$. Also $\bar{\phi}_I = n_I/\rho_0 V$, $\bar{\phi}_\pm = n_\pm/\rho_0 V$. The salt concentration C_s is related to the bulk volume fraction, $C_s = \rho_0\bar{\phi}_+/|Z_-| = \rho_0\bar{\phi}_-/|Z_+|$. The dimensionless parameter $\tau = 4\pi\rho_0 b^2 l_B = 4\pi l_B/b$ is proportional to the ratio of the Bjerrum length l_B to the Kuhn's segment size b. τ is an important scaling factor in the problem under consideration. In the expression of the mean field free-energy (1), the first integral accounts for the pairwise interactions polymer segments and solvents and the contributions from the partial mean fields for all the system components. Note, that non-electrostatic pairwise interactions of ions are neglected in this approximation. The logarithmic terms account for the translational entropy of polymer chains and all small molecules. The second integral gives the contribution from the electrostatic interactions. In SCFT, the mean fields depend on the local volume fractions, which in turn are determined by the statistical distribution of polymer conformations affected by these external fields. The details of our scheme are presented in the Appendix.[29]

The conformation statistics of chains are described by the end-integrated propagators $q(\mathbf{r}, t)$ and $q^+(\mathbf{r}, t)$. Each diblock copolymer is described by four such functions: $q_A(\mathbf{r}, t)$, $q_A^+(\mathbf{r}, t)$, $q_B^+(\mathbf{r}, t)$, and $q_B(\mathbf{r}, t)$. $q_A(\mathbf{r}, t)$ is defined as the probability of finding the end segment of A block of length t at point $\mathbf{r}$. Correspondingly, $q_A^+(\mathbf{r}, t)$ is the probability of finding the end segment of A chain of length t at $\mathbf{r}$, provided that the other end is connected to the B block. The propagators are determined by the mean field $\omega_A(\mathbf{r})$ and satisfy the modified diffusion equations:

$$\frac{\partial q_A(\mathbf{r}, t)}{\partial t} = \frac{b^2}{6}\nabla q_A(\mathbf{r}, t) - \omega_A(\mathbf{r})q_A(\mathbf{r}, t), \quad (2a)$$

$$\frac{\partial q_B(\mathbf{r}, t)}{\partial t} = \frac{b^2}{6}\nabla q_B(\mathbf{r}, t) - \omega_B(\mathbf{r})q_B(\mathbf{r}, t). \quad (2b)$$

The equations for $q_A^+(\mathbf{r}, t)$ and $q_B^+(\mathbf{r}, t)$ are identical to those for $q_A(\mathbf{r}, t)$ $q_B(\mathbf{r}, t)$ [Eq. (2a)].

The initial conditions for the propagators are determined by the connectivity. For diblock copolymers, the initial conditions are

$$q_A(\mathbf{r}, 0) = q_B(\mathbf{r}, 0) = 1, \quad q_A^+(\mathbf{r}, 0) = q_B(\mathbf{r}, N_B), \text{ and } q_B^+(\mathbf{r}, 0) = q_A(\mathbf{r}, N_A). \quad (3a)$$

The situation is slightly different for triblock copolymers, since both ends of the B block are symmetrically connected to identical A blocks. Therefore, $q_B^+(\mathbf{r}, t)$ is identical to $q_B(\mathbf{r}, t)$ and the initial conditions are

$$q_A(\mathbf{r}, 0) = 1, \quad q_A^+(\mathbf{r}, 0) = q_B(\mathbf{r}, N_B) \text{ and } q_B(\mathbf{r}, 0) = q_A(\mathbf{r}, N_A). \quad (3b)$$

The electrostatic potential coupled with the partial

densities by the Poisson–Boltzmann equation:

$$\nabla^2\varphi_e(\mathbf{r}) = -\frac{\tau}{b^2}\phi_e(\mathbf{r}) = -\frac{\tau}{b^2}[p\phi_A(\mathbf{r}) + Z_I\phi_I(\mathbf{r}) + Z_+\phi_+(\mathbf{r}) + Z_-\phi_-(\mathbf{r})]. \quad (4)$$

Equations (2)–(4), complemented with the equations relating to the partial mean fields and densities given in Appendix (A1–A14), constitute a closed set of SCFT equations, which are solved numerically. The strategy in determining the most favorable morphology assumed by the system under consideration is the following. We check, which of the possible mesophases, lamellar, gyroid, hexagonal, or body-centered cubic, would provide the lowest free-energy at given system parameters $(N, b, f_A, \bar{\phi}_C, p, \tau, \bar{\phi}_\pm, \chi_{AB}, \chi_{AS}, \chi_{BS})$ and compare it with the free- energy of the homogeneous disordered mixture (phase D) chosen as a reference state. The free- energy density [Eq. (1)] of the disordered phase reduces to the following equation:

$$\frac{F_D}{V\rho_0 k_B T} = \chi_{AB}\phi_A\phi_B + \chi_{AS}\phi_A\phi_S + \chi_{BS}\phi_B\phi_S + \frac{\bar{\phi}_p}{N}\ln\bar{\phi}_p + \sum_{i=S,I,\pm}\bar{\phi}_i\ln\bar{\phi}_i. \quad (5)$$

To this end, the SCFT equations are solved in each probe mesophase, and the calculated free- energy is minimized with respect to the mesophase spacing D. Constructing the phase diagram, we select for each point in the parameter space the morphology of the lowest free-energy.

For ordered mesophases, all functions of interest including the mean field, the mean densities, the end-integrated propagators, reflect the particular symmetry. They are periodic functions with period D, which can be developed into a series over a particular set of basis functions. The most efficient and accurate method to solve the SCFT equations is the reciprocal-space method developed by Matsen and Schick,[6] which is based on the Fourier transforms of the plane wave-like basis functions $e^{i\mathbf{G}.\mathbf{r}}$ with the reciprocal lattice vectors determined by the space symmetry group of given morphology. In particular, one constructs a set of new basis functions $g_n(\mathbf{r})$, which are the linear combinations of the plane waves accounting for the point group symmetry of the order phase.[2] An advantage of the reciprocal-space method is that upon the Fourier transformation, the second order partial differential equations are transformed into a set of coupled linear equations, which is convenient for numerical solutions.

III. RESULTS AND DISCUSSION

In this section, we demonstrate the proposed approach drawing on several instructive examples of self-assembly in polyelectrolyte melts and solutions. For simplicity, we assume that the ions are monovalent and set $Z_+ = Z_I = -Z_- = 1$ in all calculations. The dielectric constant $\varepsilon_r = 20$ was assumed in all our calculations..

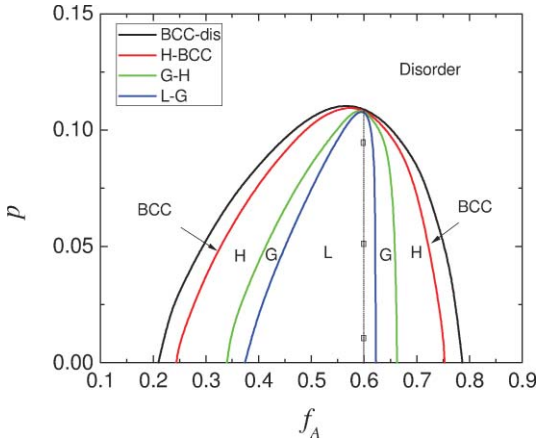

FIG. 1. Phase diagram of diblock copolymer melts $\chi_{AB} = 0.2$, $N = 100$, and $\tau = 50$. The density profiles at the states indicated by squares in the lamellar mesophase at the critical composition $f_A = 0.6$ are given in Fig. 3.

A. Diblock and triblock polyelectrolite melts

To provide a connection with previous investigations, we first consider a salt-free melt of charged-neutral AB diblock copolymer that was studied in Ref 16.The calculations were performed for diblocks composed of $N_A + N_B = N = 100$ effective Kuhn's segments of length $b = 7$Å by varying the composition $f_A = N_A/N$ from 0.1 to 0.9 and the charge density p of A blocks.

Figure 1 shows the calculated phase diagram for AB copolymer melts with the Flory mismatch interaction parameter $\chi_{AB} = 0.2$ in the composition f_A – charge density p coordinates. The reference uncharged system at $p = 0$ exhibits different mesophase morphologies depending on the composition f_A: lamellar at $0.37 < f_A < 0.62$; gyroid at $0.34 < f_A < 0.37$ and $0.63 < f_A < 0.66$; bcc at $0.21 < f_A < 0.25$ and $0.75 < f_A < 0.79$. At $0 < f_A < 0.21$ and $0.79 < f_A < 1$, the neutral system is disordered. Electrostatic interactions affect the phase behavior substantially. For example, let's consider $f_A = 0.5$ that would correspond to the critical density in the neutral diblock. At $p = 0$, it is a symmetric uncharged diblock copolymer that naturally forms a lamellar mesophase. When the charge density p reaches 0.074, the gyroid morphology becomes more stable than the lamellar, and the system makes an L-G transition. As p increases further, the system at $p = 0.086$ transits into a hexagonal mesophase where A-rich cylindrical micelles are surrounded by B-rich matrix, and then at $p = 0.1$ into a BCC mesophase with A-rich spherical micelles surrounded by B-rich matrix. At $p > 0.108$, the melt is disordered with A and B components mixed.

Overall, the transitions between the mesophases with the charge increase occur in the same sequence as the transitions in the reference neutral diblock melt with the increase of temperature or the decrease of the Flory mismatch parameter χ_{AB}. Thus, the electrostatic interactions reduce repulsion between A and B segments and make ordered mesophases less stable compared with reference neutral systems, in agreement with conclusions of the literature.[16] This effect can be explained by the action of counterions, which mix with the B-rich subphase and attract A segments of the polymers.

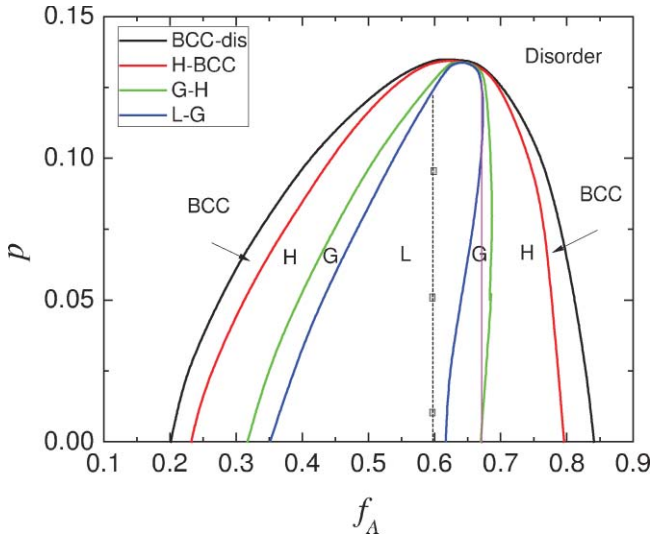

FIG. 2. Phase diagram of ABA triblock copolymer melts at $\chi_{AB} = 0.2$, $N = 200$, and $\tau = 50$. The purple vertical line at $f_A = 0.67$ shows possible transitions from hexagonal to gyroid to lamellar mesophases with the increase of charge density. The density profiles of A and B segments at the states indicated by squares in the lamellar mesophase at $f_A = 0.6$ are given in Fig. 3(b).

It is worth noting that unlike the reference neutral system, the phase diagram for charged-neutral diblock copolymer is asymmetric, so that the mesophase morphology at a certain f_A is not the inverse copy of that at $1-f_A$. The system shows a critical point at $p = 0.11 \pm 0.002$ and $f_A = 0.6 \pm 0.01$, where the free-energies of all mesophases are equal. Here, we cannot conclude whether or not this critical point reflects the true criticality in the statistico-mechanical sense. The numerical calculations of free-energy near this critical point are very time consuming and bear a significant error. However, our calculations are accurate enough to distinguish the difference of the critical point position (of ~0.6) in the given charged system from the symmetric value of 0.5 characteristic for neutral diblocks. Most likely, the critical point displayed in Fig. 1 is similar to the critical point in the Leibler's mean field theory and SCFT of asymmetric neutral diblock melts with the charge density playing a destabilizing role, similar to the reciprocal Flory parameter $1/\chi_{AB}$ or temperature.[7–9,12]

The phase diagram of salt-free ABA triblock copolymer melts is given in Fig. 2. The length of chain is $N = 200$ with Flory parameter $\chi_{AB} = 0.2$. Similarly to the case of AB diblock copolymer melts, the increase of charge density p of A blocks plays a "disordering" role similar to the increase of temperature or the decrease of AB nonelectrostatic repulsion. However, ABA triblock polyelectrolytes show a higher stability and the order–disorder transitions happen at higher charge densities compared to AB diblocks. This is confirmed with sharper density profiles shown in Fig. 3, right. This stabilizing effect may be related to the fact that since the triblock chain has two end A blocks, the increase of change density increases the repulsion between end blocks of the same chains, which make segregated morphologies more stable.

Since the neutral symmetric ABA triblock copolymer melt is characterized by an asymmetric phase diagram[9] as a result of the broken symmetry between A and B blocks, one could expect that electrostatic interactions would further increase the phase diagram asymmetry. Indeed, the ABA triblock phase diagram in Fig. 2 is even more asymmetric than the one in Fig. 1 for AB diblocks. Moreover, in a certain range of compositions, the phase diagram for charged triblock exhibits unexpected features, allowing the increase of charge for the transitions from hexagonal to gyroid to lamellar mesophases, as shown by the vertical purple line at $f_A = 0.67$ in Fig. 2.

In Fig. 3, we present the distribution of volume fractions of A segments over one period of the lamellar phase for diblock (left) and triblock (right) copolymer melts with the composition $f_A = 0.6$, which corresponds to the critical point of the diblock phase diagram, see Fig. 1. The density profiles show distinct A-rich and B-rich regions. If A block acquires a positive (or negative) charge and counterions spread over the system, the density profiles gradually smear out with the increase of the charge density, which implies that A and B block become more miscible. This result confirms that charges decrease the effective degree of segregation. Also, this figure shows that an increase in charge density of A blocks affects diblock melts more significantly than triblock melts. Thus, we may conclude that the triblock copolymer lamellar have a higher resistance to instability induced by electrostatic effects compared to diblock copolymers. The possible reason is the importance of bridge conformations. The charges on A blocks

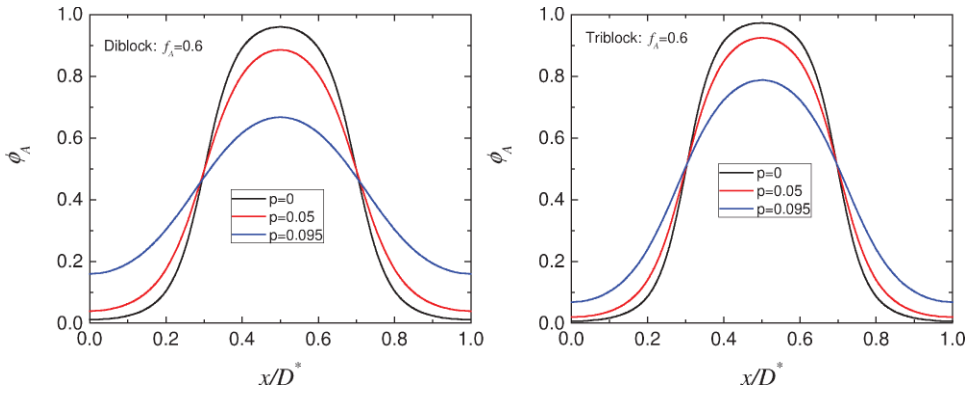

FIG. 3. The volume fraction of A segment of diblock (left) and triblock (right) copolymer melts at different charge densities. The calculations correspond to the system shown in Figs. 1 and 2 at $f_A = 0.6$ that corresponds the lamellar phases at the points on dashed lines in Figs. 1 and 2.

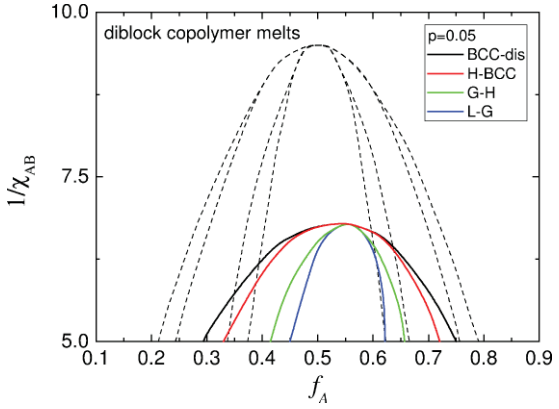

FIG. 4. Phase diagram of AB diblock copolymer melt as a function of the composition f_A and the inverse of the Flory mismatch interaction parameter, $1/\chi_{AB}$. Solid lines represent the phase boundaries for the charged copolymer at $p = 0.05$; dashed lines correspond to the neutral system ($p = 0$). The chain length $N = 100$; $\tau = 50$. The low limit of $1/\chi_{AB} = 5$ corresponds to the cross section of the phase diagram presented in Fig. 1 at $p = 0.05$. The polyelectrolyte phase diagram is asymmetric in contrast with that of the neutral diblock. The critical point, $f_A = 0.55$, $\chi_{AB} = 0.148$ ($1/\chi_{AB} = 6.77$), for the polyelectrolyte shifts to smaller χ_{AB} and larger f_A compared to the neutral diblock critical point, $f_A = 0.50$ and $\chi_{AB} = 0.105$ ($1/\chi_{AB} = 9.5$).

induce the repulsion between the end blocks of the bridging chains that make ordered structures more stable.

To confirm our conclusion that the charge density increase affects the mesophase stability boundary in the same direction as the decrease of the Flory mismatch parameter χ_{AB}, we present in Figs. 4 and 5 the phase diagrams obtained by varying χ_{AB} at the fixed charge for diblock triblock copolymer melts, respectively. Comparing the presented phase diagrams for charged ($p = 0.05$) and neutral copolymers, one can find that increasing the charge of A block in both the diblock and triblock copolymers causes the shift of the phase transition lines toward lower $1/\chi_{AB}$ value (or higher mismatch parameters χ). The most instructive observation made from this comparison is that while the critical point for neutral copolymers, both diblocks and triblocks, is at $f_A = 0.5$, the critical point for polyelectrolytes takes place at a higher fraction of charged blocks, $f_A > 0.5$, which results from the broken symmetry between A and B blocks due to the electrostatic interactions.

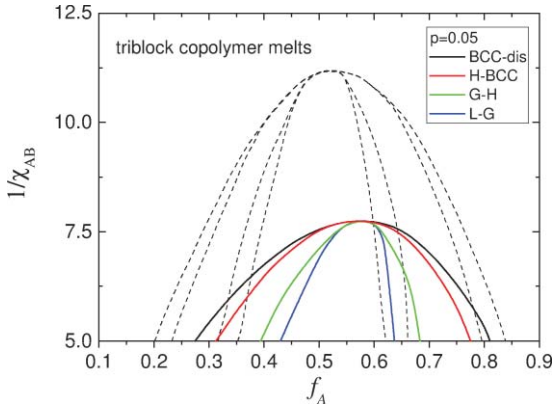

FIG. 5. Phase diagram of ABA triblock copolymer melt as a function of the composition f_A and the inverse of Flory mismatch interaction parameter $1/\chi_{AB}$. The chain length is $N = 200$; other parameters are the same as in Fig. 4. The low limit of $1/\chi_{AB} = 5$ corresponds to the cross section of the phase diagram presented in Fig. 2 at $p = 0.05$. The polyelectrolyte phase diagram is more asymmetric than that of the neutral triblock. The critical point, $f_A = 0.58$, $\chi_{AB} = 0.13$ ($1/\chi_{AB} = 7.72$), for the polyelectrolyte shifts to smaller χ_{AB} and larger f_A compared to the neutral diblock critical point, $f_A = 0.50$ and $\chi_{AB} = 0.09$ ($1/\chi_{AB} = 11.1$).

To the best of our knowledge, the complete SCFT phase diagrams of diblock and triblock polyelectrolytes in the composition-charge density plane, such as given in Figs. 1 and 2, are presented for the first time. In the earlier work of Kumar and Muthukumar,[16] SCFT was employed only for consideration of lamellar structures in diblocks. Although their RPA calculations in other ordered morphologies gave a valuable insight onto the role of electrostatic interactions, the results cannot be considered as precise as the SCFT results, especially for the states far from the stability limit, due to an inherent deficiency of RPA compared to SCFT.

B. Triblock copolymer in salt solution

Modeling block polyelectrolytes in salt solutions is more computationally challenging than modeling block polyelectrolytes melt due to a larger number of components. Also, the salt concentration C_s and the polymer density ϕ_C extend the number of important parameters that determine the system morphology. Self-assembly of block polyelectrolytes in aqueous solutions was simulated with DDFT.[21,30–33] To demonstrate a feasibility of SCFT, we considered $A_3B_9A_3$ triblock aqueous solution studied earlier by Kyrylyuk and Fraaije.[21] The Flory interaction parameters in this system are $\chi_{AB} = 3$, $\chi_{AS} = 1.4$, and $\chi_{BS} = 1.7$. This means that not only hydrophobic B block but also A block in the neutral (nondissociated) form would be immiscible with water. The Kuhn's segment length $b = 15$Å, the dielectric constant of the entire system is $\varepsilon_r \approx 20$, and the concentration of 1–1 NaCl electrolyte is $C = 100$ *mM*.

In Fig. 6, we present a phase diagram of the triblock copolymer solution in the polymer concentration ϕ_C – charge density p plane. In the range of polymer concentration $0.5 < \phi_C < 0.7$, the ordered mesophases (lamellar, hexagonal,

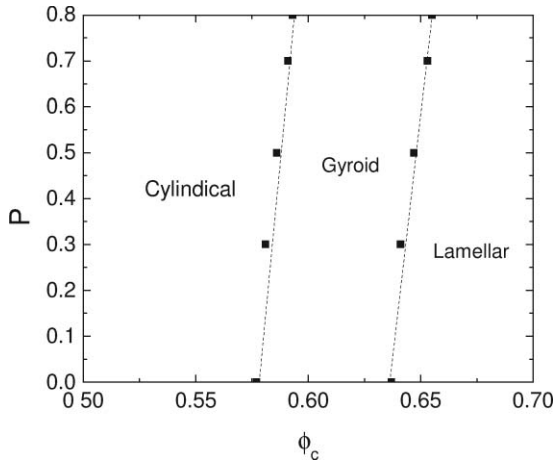

FIG. 6. The phase diagram of triblock polyelectrolyte ($A_3B_9A_3$) solution in ϕ_C and p parameter space at $\chi_{AB} = 3$, $\chi_{AS} = 1.4$, $\chi_{BS} = 1.7$. The polymer accepts cylindrical hexagonal, bicontinuous gyroid, or lamellar morphology.

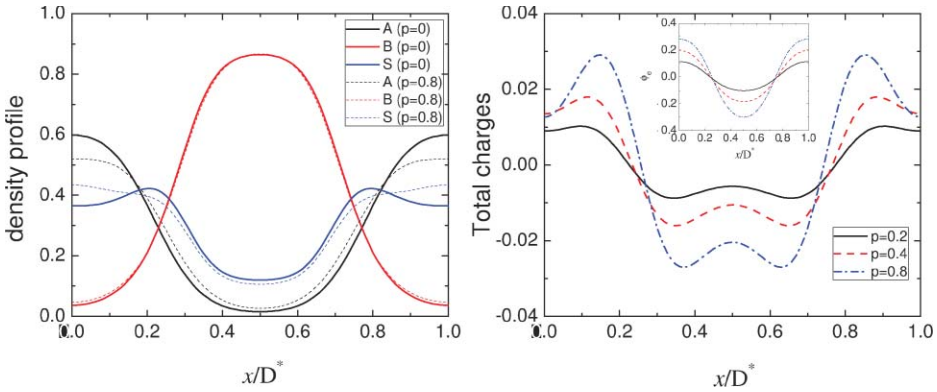

FIG. 7. The density profiles of triblock polyelectrolyte ($A_3B_9A_3$) solution in a lamellar mesophase spacing with $\phi_C = 0.7$ at different charge fraction of A block. The Flory parameters are $\chi_{AB} = 3$, $\chi_{AS} = 1.4$, and$\chi_{BS} = 1.7$. Left figure gives the densities for A, B, and S with $p = 0$ (solid lines) and $p = 0.8$ (dashed lines). Left figure gives the total charge distribution at $p = 0.2$, 0.4, and 0.8. The inset figure gives the corresponding electrostatic potentials.

and gyroid) in the system under consideration are favored over the uniform disordered solution, since the free-energy difference between ordered and disorder morphologies is negative. For uncharged and charged systems, the consequent transitions from hexagonal to gyroid and then to lamellar mesophases occur as the polymer density increases. The polymer densities corresponding to these transitions depend on the charge density—the larger the charge density the larger the transition polymer density. This trend agrees qualitatively to that obtained with DDFT.[21] Quantitatively, the results of DDFT and SCFT calculations deviate substantially. SCFT showed a weaker dependence of the transition points on the charge density, and the system exhibited an ordered morphology in the entire range of the charge densities considered, while the authors[21] observed order–disorder transitions with the increase of charge density. A possible reason for that is the use of the Donnan approximation in Ref. 21, which overestimates the entropic contribution from the small ions to the system free-energy.

The density profiles in the lamellar mesophase at different charge densities are shown in Fig. 7. The increase of charge density of A block hardly affects the density of the hydrophobic block B, but it influences the distribution of the solvent components and A segments. Additional charges cause more A segments to transfer from A-rich region to B-rich region because of the increasing electrostatic repulsion between A segments. Also, more solvent molecules are transferred to A-rich regions. Thus, the charges decrease the mismatch between A and B blocks, as it is characteristic to polyelectrolyte melts. Comparing the total charge distributions at different charge densities, we may conclude that with the increase of charge density, the small ions redistribute and form a sharper total charge density profile, which results in the increase of the interfacial tension between A-rich and B-rich domains and, consequently, in the increase of the system free-energy.

IV. DISCUSSION AND CONCLUSIONS

The mean field phase diagrams constructed for diblock and triblock polyelectrolyte melts in the composition-charge density plane at a fixed Flory mismatch parameter χ_{AB} resembling the phase diagrams for neutral asymmetric block copolymers in the composition $-1/\chi_{AB}$ plane. The constructed diagrams have the critical point, at which the mesophase stability boundaries coincide. At the critical composition, the order–disorder transition with the increase of charge density occurs directly from the lamellar mesophase without intermediate order–order L-G, G-H and H-BCC transitions, which are otherwise required. Thus, an increase of electrostatic interactions plays the same role as a decrease of the block mismatch and facilitates mesophase disordering. The phase diagrams for polyelectrolyte diblocks and tribocks in the composition $-1/\chi_{AB}$ plane are asymmetric with the critical point shifted toward larger f_A and smaller χ_{AB} values compared to the neutral block copolymers with symmetric critical point at $f_A = 0.5$.

At the current state of development, this theory, as well as all other attempts to model self-assembly in polyelectrolyte system, contains a serious flaw, which is hidden under the assumption that the interactions between counterions and other components are limited to the electrostatic interactions. This assumption implies that the volume of counterions is neglected and they do not contribute to Flory–Huggins pairwise interactions. The disordering effect of electrostatic interactions predicted by the SCFT model is caused by the translational entropy of the counterions, which, for the lack of own volume, are allowed to flow freely between the hydrophilic and hydrophobic subphases. In reality, counterions do have preferences, and they are typically strongly hydrophilic that makes them to remain in the aqueous subphase. In this case, the translational entropy effect may be insignificant in experiments. Nevertheless, the results of this study seem to agree with some experimental findings that charged-neutral diblock and triblock copolymers show less ordering than the respective neutral copolymers. For example, distinct hexagonal and lamellar morphologies were observed in neutral (nonsulfonated) polystyrene — poly(rthylene-butadiene) diblock and polystyrene — poly(rthylene-butadiene) — polystyrene triblock colopymers known as SEBS.[34] Most of the published studies of sulfonated SEBS reported strong segregation in these systems but with an irregular morphology.[26] In their study of the structure of triblock copolymers using

atomic force microscopy, Gromadzki *et al.*[35] observed uniform structures in sulfonated polyethylene–polystyrene diblock copolymers. Spherical micellar formations were found at high hydration and referred to the regions with high concentration of sulfonic acid groups. Disordering of the sulfonated SEBS triblock copolymer solution with the increase of the degree of sulfonation was reported in Ref. 36. However, distinct lamellar morphology of SEBS films was found by Elabd *et al.*[37] Recent comprehensive study of Park and Balsara[38] reported a wide range of different ordered structures in sulfonated PS-polymethylbuty diblocks of different degree of sulfonation. Although it appears that the structure changes from L to G and subsequently to H as the sulfonation increases, it should be noted that the effective repulsion between the blocks also changes with sulfonation, while in our work the mismatch parameter χ_{AB} was kept constant independently of the charge density p.

Another important problem lies in the very definition of ordering. In SCFT, the regular geometry of the system is specified in advance, and the free-energies of different morphologies are calculated and compared at given conditions. The morphology that has the lowest free-energy is expected to be formed in the equilibrated system. The free-energies of ordered mesophases (lamellar, gyroid, hexagonal, and BCC) are compared with that of the homogeneous solution with uniformly distributed components, which are considered as the disordered phase. Thus, a variety of heterogeneous and "semi-ordered" structures, which are frequently observed in experiments and dynamic simulations, where no particular order (beyond the periodic boundary conditions in simulations) is imposed on the system, falls out of the SCFT consideration. In reality, disordered morphology should mean that no particular symmetry is formed, but the system may be strongly nonuniform and contain, for example, micelles arranged without any particular symmetry.

Further development of the proposed model should target particular experimental systems and subsequent comparison with experimental data (which, probably, are not available with a required precision so far) in order to clarify the specifics of the influence of electrostatic interactions on the segregation morphology in polyelectrolyte systems.

ACKNOWLEDGMENTS

This work was supported by DTRA Grant No. HDTRA 1-08-1-0042.

[1] F. S. Bates and G. H. Fredrickson, Phys. Today **52**(2), 32 (1999).
[2] *Developments in Block Copolymer Science and Technology*, edited by Hamely (Wiley, New York, 2004).
[3] T. Nakanishi, S. Fukushima, K. Okamoto, M. Suzuki, Y. Matsumura, M. Yokoyama, T. Okano, Y. Sakurai, and K. Kataoka, J. Controlled Release **74**, 295 (2001).
[4] N. W. Deluca and Y. A. Elabd, J. Polym. Sci., Part B: Polym. Phys. **44**, 2201 (2006).
[5] G. H. Fredrickson, *The Equilibrium Theory of Inhomogeneous Polymers* (Oxford University Press, New York, 2006).
[6] M. W. Matsen and M. Schick, Phys. Rev. Lett. **72**, 2660 (1994).
[7] L. Leibler, Macromolecules **13**, 1602 (1980).
[8] A. M. Mayes and M. O. de la Cruz, J. Chem. Phys. **91**, 7228 (1989).
[9] M. W. Matsen and R. B. Thompson, J. Chem. Phys. **111**, 7139 (1999).
[10] M. W. Matsen, J. Chem. Phys. **113**, 5539 (2000).
[11] M. W. Matsen and M. Schick, Macromolecules **27**, 4014 (1994).
[12] M. W. Matsen and F. S. Bates, J. Polym. Sci., Part B: Polym. Phys. **35**, 945 (1997).
[13] G. H. Fredrickson and E. Helfand, J. Chem. Phys. **87**, 697 (1987).
[14] A. M. Mayes and M. O. de la Cruz, J. Chem. Phys. **95**, 4670 (1991).
[15] J. F. Marko and Y. Rabin, Macromolecules **25**, 1503 (1992).
[16] R. Kumar and M. Muthukumar, J. Chem. Phys. **126**, 214902 (2007).
[17] A. C. Shi and J. Noolandi, Macromol. Theory Simul. **8**, 214 (1999).
[18] Q. Wang, T. Taniguchi, and G. H. Fredrickson, J. Phys. Chem. B **108**, 6733 (2004).
[19] A. Jusufi, A. P. Hynninen, and A. Z. Panagiotopoulos, J. Phys. Chem. B **112**, 13783 (2008).
[20] M. Banaszak and J. H. R. Clarke, Phys. Rev. E **60**, 5753 (1999).
[21] A. V. Kyrylyuk and J. Fraaije, J. Chem. Phys. **121**, 2806 (2004).
[22] P. V. Komarov, I. N. Veselov, P. P. Chu, P. G. Khalatur, and A. R. Khokhlov, Chem. Phys. Lett. **487**, 291 (2010).
[23] Y. Rabin and J. F. Marko, Macromolecules **24**, 2134 (1991).
[24] E. Helfand and Z. R. Wasserman, Macromolecules **9**, 879 (1976).
[25] M. W. Matsen, J. Chem. Phys. **102**, 3884 (1995).
[26] J. Won, S. W. Choi, Y. S. Kang, H. Y. Ha, I. H. Oh, H. S. Kim, K. T. Kim, and W. H. Jo, J. Membr. Sci. **214**, 245 (2003).
[27] M. Doi and S. F. Edwards, *The Theory of Polymer Dynamics* (Oxford University Press, New York, 1986).
[28] E. Helfand, J. Chem. Phys. **62**, 999 (1975).
[29] See supplementary material at http://dx.doi.org/10.1063/1.3532831 for a detailed description of the closed set of SCFT equations for determining free-energies of ordered mesophases.
[30] Y. R. Zhao, X. Chen, and G. D. Zhang, J. Dispersion Sci. Technol. **29**, 1331 (2008).
[31] S. H. Yang, S. L. Yuan, X. Q. Zhang, and Y. J. Yan, Colloids Surf. A **322**, 87 (2008).
[32] S. H. Yang, X. Q. Zhang, and S. L. Yuan, J. Mol. Model. **14**, 607 (2008).
[33] S. L. Yuan, X. Q. Zhang, G. Y. Xu, and D. J. Zhang, J. Mol. Model. **12**, 406 (2006).
[34] B. Heck, P. Arends, M. Ganter, J. Kressler, and B. Stuhn, Macromolecules **30**, 4559 (1997).
[35] D. Gromadzki, P. Cernoch, M. Janata, V. Kudela, F. Nallet, O. Diat, and P. Stepanek, Eur. Polym. J. **42**, 2486 (2006).
[36] X. Y. Lu, W. P. Steckle, and R. A. Weiss, Macromolecules **26**, 6525 (1993).
[37] Y. A. Elabd, C. W. Walker, and F. L. Beyer, J. Membr. Sci. **231**, 181 (2004).
[38] M. J. Park and N. P. Balsara, Macromolecules **41**, 3678 (2008).